Global Journal of Engineering and Technology Advances
eISSN: 2582-5003
Cross Ref DOI: 10.30574/gjeta
Journal homepage: https://gjeta.com/

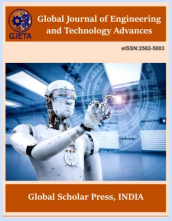

(RESEARCH ARTICLE)

Check for updates

Multi and single epipolar geometry-based filters vs. affine and conformal 2D transformation-based filters

Mustafa M. Amami *

Department of Civil Engineering, Benghazi University, Benghazi, Libya.

Global Journal of Engineering and Technology Advances, 2022, 10(03), 032–051

Publication history: Received on 04 February 2022; revised on 11 March 2022; accepted on 13 March 2022

Article DOI: https://doi.org/10.30574/gjeta.2022.10.3.0047

Abstract

The accuracy of Optical Robot Navigation (ORN) depends mainly on the quality of the Automatic Image Matching (AIM) results. Conformal 2D transformation-based Filter (C-2DF), affine 2D transformation-based Filter (A-2DF) and Single Epipolar Geometry-based Filter (S-EGF) are common filters used in ORN. Multi-Epipolar Geometry-based Filter (M-EGF) has been introduced, tested and evaluated by the author and compared by each filter of those mentioned above in separate research papers. This paper comes to include all these individually comparisons, with additional details, showing the advantages and limitations of all filters comparing to each other. Tests show that C-2DF and A-2DF have failed to deal with AIM results in areas with open, narrow, and confused DOF. Also, they have failed to find out the right mathematical model in data with high rate of mismatched points and data obtained from images with difficult view angles. With limited DOF and low rate of errors, C-2DF and A-2DF have provided relatively sufficient results, which can be used for ORN applications that do not require precision. A-2DF is relatively better than C-2DF due to its flexibility to deal with figures including different scales, which is the case when dealing with different levels of DOF and different capturing angles between the cameras. The processing time is another disadvantage of C-2DF and A-2DF, where these are based on iterative estimation methods. Tests display how A-2DF is slowest, which keeps it away from using with real time ORN applications.

Tests show that S-EGF and M-EGF are timesaving and able to deal with any AIM results, regardless the DOF, view angle and errors rate in observations. S-EGF is affected in areas including lines parallel to the cameras base line. M-EGF has offered the best results in terms of providing error-free filtered matched points in all tests. This can be attributed to the high restriction level of this filter, where the probability for the mismatched point to pass throughput the three co-planarity equations is nearly zero. M-EGF and S-EGF are affected by the quality of the Interior Orientation Elements (IOEs) and Exterior Orientation Parameters (EOPs) of the three cameras, leading to rejection a small number of corrected matched points, which can be avoided with professionally manufactured ORN systems. Tests illustrated that S-EGF and M-EGF are extremely high-speed and S-EGF is the faster and M-EGF, C-2DF, and A-2DF comes after, respectively. All results indicated that M-EGF is the best, as it is fast, restricted, reliable, and error-free technique and is suitable for real-time precise ORN applications.

Keywords: Multi and Single Epipolar Geometry; Affine and Conformal 2D Transformation; Automatic Image Matching; SLAM; Optical Robot Navigation

1. Introduction

Photogrammetry can be simply defined as a science of obtaining reliable information about physical objects from photographic images. Analytical photogrammetry describes the mathematical relationships between camera IOEs, EOPs, measured photo coordinates, ground control points (GCP), and Object Space Coordinate (OSC). Co-linearity

* Corresponding author: Mustafa M. Amami
Department of Civil Engineering, Benghazi University, Benghazi, Libya.

condition equations are the most famous mathematical formula used in photogrammetric relative and absolute applications, including Space Resection (SR), Space Intersection (SI), Bundle Block Adjustment (BBA), and Self-Calibration Bundle Block Adjustment (SCBBA) [1]. ORN is the technique by which robot can be localized and oriented relatively to the surrounding environment in stationary and moving cases using optical sensors. ORN is integration between photogrammetry and computer vision, where photogrammetry provides the mathematical bases of optical navigation, and computer vision works on extracting the corresponding points on images automatically [2]. ORN in photogrammetric subjects is referred to as vision-based navigation and image-based navigation, and in computer science as Simultaneous Localization and Mapping (SLAM). SLAM is more general and comprehensive, as it includes optical and laser scanning based navigation [3]. At present, robots, based on ORN, are used extensively in many areas, including security, medical, and engineering applications and this subject is experiencing rapid development and witnessing a great demand in the global labor market [4]. Figure (1) shows examples of ORN applications.

Figure 1 ORN applications in security, medical and engineering areas from left to right

In ORN, robot, provided with two or more cameras starts in unidentified environment with unknown position and orientation. The cameras, which are adjusted to have wide overlapping viewing areas, take images simultaneously. Computer vision works on matching the images automatically, finding out the corresponding points. As the relative orientation parameters between the robot cameras are known, one camera can be fixed with zero values and the other camera/s can be localized and oriented relatively to this camera. As the EOPs and IOEs of all cameras become known, and the image points are ready, OSC can be determined relatively using SI. BBA and SCBBA can also be used if the relative EOPS of the cameras (except the main fixed one) have been used as observations with standard deviations, where all observations can be bundled together giving the adjusted values of used observations and relative OSC of the image matched points. Moving to the next station, the cameras takes new images, which are matched with those of the previous station, finding out common points and the image coordinates of the relative OSC in the new images. In this station, EOPs of all cameras are unknown relative to the reference points and orientations. However, a number of OSC in the images of the second station are known, which can be used to determine the EOPs of all cameras using SR. Also, BBA and SCBBA can also be used if the relative OSC have been used as observations with standard deviations, where all observations can be bundled together giving the adjusted values of used observations and relative EOPs of the cameras. Theoretically, ORN can be carried out in relative coordinate system and when necessary, at least three GCPs can be used for absolute positioning. As seen, ORN is based mainly on two steps: localization which is represented in SI, and mapping which is represented in SR, and the quality of the results of these two procedures are mainly based on the precision of image coordinates and the quality of matching the corresponding points between images [5, 6]. Figure (2) illustrates ORN technique workflow.

Finding out the corresponding points on the overlapping areas of multiple images is part of many photogrammetry and computer vision applications, such as image registration, camera calibration, object detection, and image recovery. Several different methods have been introduced for AIM, which can be classified into three categories, namely: area-based, feature-based, and relation-based matching. Cross-correlation and least squares correlation are the most common techniques used for matching the detected common points between images. AIM, in general, includes three main steps. In the first, the interest points in each image are selected at distinctive locations, such as corners, edges, blobs, and T-junctions. Repeatability is regarded as the most important property of any an interest point detector, where it reflects the detector reliability for finding the same physical interest points under different viewing conditions. After that, the neighborhood of each selected interest point is represented by a feature vector. For successful AIM, the descriptor should be distinctive and robust to: noise, detection displacements and geometric and photometric

deformations. In the last step, the calculated descriptor vectors of the different points are matched based on a distance between the vectors, e.g. the Mahalanobis or Euclidean distance. The dimension of the descriptor plays a significant role in the processing time, where less dimensions are recommended for fast AIM, and in contrast, using lower dimensional feature vectors leads to less distinctive descriptor, resulting degraded outputs [5, 7, 8]. Scale Invariant Feature Transform (SIFT) [9], Principal Component Analysis (PCA)–SIFT [10], and Speeded Up Robust Features (SURF) [11] are considered to be from the most common robust feature detection techniques used in photogrammetry and computer vision applications [12].

Figure 2 ORN technique workflow

Speeding up AIM and precision of detecting corresponding points between images are the two main keys of successful ORN, where the whole procedure is carried out in real time. For speeding up image matching processing, image pyramid and integral image techniques can be used, reducing the processing time significantly. Integral image is an intermediate image representation computed rapidly from an input image by the sum of the intensity values between the point and the origin, which helps to accelerate the time of any upright rectangular calculation [5, 6]. As AIM methods use Mahalanobis distance and correlation techniques for comparing the descriptors of common points and finding out the corresponding points, mismatching is highly expected, especially in environments with similar and repeated features. Identifying outliers is very important in ORN, as automation is used for measuring and determining the observations, and there is no opportunity for checking and investigating the data manually for gross errors. Outliers for multiple measurements of a single quantity can be detected easily using the normal distribution of the observational errors, which is not the case in ORN, where single measurements are fitted together during LSM computations.

For precise and robust automatic detection of mismatched points, a mathematical relationship including the matched points across the two images should be known. There are two types of mathematical relationships that can be used for

filtering the automatic mismatched points of stereo image pair: image points-independent models, and image points-dependent models. In independent models, image points are used in the model as inputs and all parameters in the model are known, thus, there is no need for parameters estimation. Independent models with no redundancy, such as co-planarity and co-linearity conditions, can be applied directly on the image points and certain threshold values are required for detecting outliers. In image points-dependent models, such as two-dimensions transformation, parameters are unknown and have to be estimated firstly from the image points that are required to be filtered, and then applied on the these points for outliers detection [2].

Random Sample Consensus (RANSAC) is a famous iterative technique that can be used for estimating mathematical model parameters from a set of observations that includes outliers. It is a non-deterministic technique that can provide results with a certain probability level, which depends mainly on the allowed number of iterations. RANSAC requires a set of observations, a clear mathematical model that link the observations, and certainty and flexibility ranges. RANSAC technique is basically include two iteratively repeated steps. In the first step, a minimum number of observations, required for determining the mathematical model parameters, is selected randomly from the whole observations. Then, the model parameters are computed using only the selected observations. As no redundancies are available, single solution can be obtained without any statistical information for evaluating the used observations. In the second step, the mathematical model with the parameters determined in step one is used with all other observations in the dataset. Based on that, observations will be divided into two groups, one for those fit the model within the allowable threshold values, and the other group includes the observations that do not fit the model and considered as outliers. Then, step one is repeated using the observations in the group of outliers, and the procedure continues until the number of observations in outlier group becomes less than the minimum number of observations required for calculating the model parameters. The final results of applying RUNSAC is a number of groups, each one has its individual calculated model parameters and the observations that fit the inputted mathematical model using these parameters. The parameters of the group that has the highest number of observations is regarded as the fit model, and its observations are inliers, whereas all other observations in the other groups are considered as outliers [3, 4].

With unlimited or significant iteration number, RANSAC has the advantage of providing reliable results even with observations that include a reasonably number of outliers, and the probability of obtaining a reasonable model increases with increasing the number of iterations. However, increasing the number of iterations makes the technique time consuming and using limited iterations affects the quality of the obtained solution, and in some cases, the optimal solution may not be obtained at all. Another disadvantage of RANSAC is the need of initial threshold values for detecting outliers, which should be carefully estimated, as small thresholds may make the model reject observations when they should be accepted and vice versa. To overcome this problem, maximum reasonable thresholds are used to guarantee including all right observations that fit the optimal model as well as the close outliers, and rejection all faraway and significant outliers. Then, LSM is used with these observations to calculate the best fit model parameters and outlier detection techniques, such as Data Spoofing Method (DSM) can be applied for detection the rest of outliers based on LSM statistical testing information [2, 3, 4].

2. Mathematical Models

2.1. 2D Conformal Transformation-Based Filter (C-2DF)

Two-dimensional transformation models are in general suitable for the automatic detection of mismatched image points, where the coordinate systems tend to lie on plane surfaces in normal circumstances. A conformal transformation is one of the main two-dimensional transformation models, in which true shape is preserved after the transformation. A conformal transformation can deal with changing in rotation, scale, and translation. At least, two points must be known in both arbitrary and final coordinate systems to apply this transformation model and find out the four main transformation parameters, namely: scale, rotation angle and 2D displacements. Conformal transformation model can be carried out in three steps, starting with scaling, then rotating, and ending with 2D translation. For more precise results, the two points used in transformation procedure should be chosen as far away from each other as possible. More than two points can be used in conformal transformation by applying LSM, providing more reliable and robust results and useful statistical testing information for detecting and removing outliers in observations. In automatic detection of mismatched points, conformal transformation can be used with RUNSAC technique, where the model parameters should be estimated firstly using the minimum number of points (two points), and then applied on the other points to check if they fit these calculated parameters. Observations that do not fit the model are listed in group of outliers. The procedure is then repeated again with another two pints from the outliers group and continues until distributing the whole points into groups, each one has its model parameters and the fitted observations. The winner model is that includes the more observations. As mentioned in the introduction, RUNSAC with reasonable maximum threshold values is used firstly and then, LSM is applied on the observations of the winner group to estimate the best fit

parameters and removing the close undetected outliers based on the obtained statistical testing information. After removing these outliers, the remain observations can be bundled again for final parameters estimation [1]. The mathematical model of C-2DF using RUNSAC and followed by LSM for any number of points (n) can be illustrated in the following steps and equations: (All equations are after [3])

2.1.1. RUNSAC "Step 1"

Choosing two random points in image (1) and there corresponding points in image (2) as the minimum number of observations used for determining the model parameters. Eqs. (1.1 to 1.4) show the mathematical model of 2D conformal transformation.

$$E_{(A)} = a * X_{(A)} - b * Y_{(A)} + T_{(E)} \quad (1.1)$$

$$N_{(A)} = a * Y_{(A)} + b * X_{(A)} + T_{(N)} \quad (1.2)$$

$$E_{(B)} = a * X_{(B)} - b * Y_{(B)} + T_{(E)} \quad (1.3)$$

$$N_{(B)} = a * Y_{(B)} + b * X_{(B)} + T_{(N)} \quad (1.4)$$

Where,

$$a = S * \cos(\alpha) \quad (2.1)$$

$$b = S * \sin(\alpha) \quad (2.2)$$

$$S = (a^2 + b^2)^{0.5} \quad (2.3)$$

$$\alpha = \tan^{-1}(b/a) \quad (2.4)$$

And,

$T_{(E)}$, $T_{(N)}$: Displacement parameters of 2D conformal transformation
S: Scale changing
A: Rotation angle
$X_{(A)}$, $Y_{(A)}$, $X_{(B)}$, $Y_{(B)}$: The coordinates of points (A) & (B) in X-Y coordinate system
$E_{(A)}$, $N_{(A)}$, $E_{(B)}$, $N_{(B)}$: The coordinates of points (A) & (B) in E-N coordinate system

2.1.2. RUNSAC "Step 2"

Testing the rest of the whole matched points with this determined model, and classifying the points into two groups: inliers, that fit the model within the allowable threshold values, and outliers, that do not do.

2.1.3. RUNSAC "Step 3"

Back to step (1), where new two points are selected randomly from the outliers group of step (2). The procedure is continued until: the specified number of iterations is finished, getting the model parameters with the maximum required number of fitted points, or the number of points in outlier group is less than that required for calculating new model parameters. The final results of RUNSAC is a number of groups, each one includes the observations that fit to a specific set of parameters of conformal 2D transformation model and the chosen group is that includes the highest number of fitted points.

2.1.4. LSM "Step 1"

As RUNSAC solution is expected to have outliers due to the reasonable maximum threshold values, that used for avoiding rejection observations when they should be accepted, the whole points in the "winner" group are used again in LSM for determining the model parameters, and computing the residuals and the standard deviation of each observation from the covariance matrix of residuals. Eqs. (3.1 to 3.6) show 2D conformal transformation observation equations with redundancy and residuals are included to make them consistent:

$$E_{(A)} + V_{E(A)} = a * X_{(A)} - b * Y_{(A)} + T_{(E)} \quad (3.1)$$

$$N_{(A)} + V_{N(A)} = a * Y_{(A)} + b * X_{(A)} + T_{(N)} \quad (3.2)$$

$$E_{(B)} + V_{E(B)} = a * X_{(B)} - b * Y_{(B)} + T_{(E)} \quad (3.3)$$

$$N_{(B)} + V_{N(B)} = a * Y_{(B)} + b * X_{(B)} + T_{(N)} \quad (3.4)$$

$$E_{(n)} + V_{E(n)} = a * X_{(n)} - b * Y_{(n)} + T_{(E)} \quad (3.5)$$

$$N_{(n)} + V_{N(n)} = a * Y_{(n)} + b * X_{(n)} + T_{(N)} \quad (3.6)$$

Where,

$T_{(E)}$, $T_{(N)}$, S , α	As above
$X_{(A)}$, $Y_{(A)}$, ……$X_{(n)}$, $Y_{(n)}$	The most probable computed values (error-free values)
$E_{(A)}$, $N_{(A)}$, ……$E_{(n)}$, $N_{(n)}$	Observed values including errors

Here, it is important to note that the residuals have been used just for E-N system coordinates, and this means that X-Y system coordinates are error-free observations. This means that even if there are errors in X-Y system coordinates, these errors will be reflected on the residuals of E-N system coordinates. In AIM, mismatching is highly expected in the two images, especially in difficult matching environments, thus, errors in all observations should be included and all observations are bundled together for precise and robust results. For applying this, it should be known that equations, in general, could be written in one of the three following forms of Eqs. (4.1 to 4.3), which are known as observation, condition and combined equations, respectively, where *(Xt)* and *(Lt)* terms for unknowns and observations, in this order.

$$F(Xt) = Lt \quad (4.1)$$

$$F(Lt) = 0 \quad (4.2)$$

$$F(Xt, Lt) = 0 \quad (4.3)$$

The observation equation is an equation including only one observation and any number of parameters. In the case of condition equation, the equation includes just observations and it is a parameter free. When the equation includes parameters and more than one observation like in 2D conformal transformation, it is defined as combined equation. However, as developed in Eqs. (3.1 to 3.6), the observation equation can also be adjusted to deal with the combined cases, where only one observation is used in each equation and the other observations in the equation are considered to be error-free. Then, an individual observation equation is added for each observation (that is considered as error-free) as developed in Eqs. (5.1 to 5.6), where each equation includes the observed and the most probable values of the observation.

$$X_{O(A)} + V_{(Xo(A))} = X_{(A)} \quad (5.1)$$

$$Y_{O(A)} + V_{(Yo(A))} = Y_{(A)} \quad (5.2)$$

$$X_{O(B)} + V_{(Xo(B))} = X_{(B)} \quad (5.3)$$

$$Y_{O(B)} + V_{(Yo(B))} = Y_{(B)} \quad (5.4)$$

$$X_{O(n)} + V_{(Xo(n))} = X_{(n)} \quad (5.5)$$

$$Y_{O(n)} + V_{(Yo(n))} = Y_{(n)} \quad (5.6)$$

Where,

$X_{O(A)}$, $Y_{O(A)}$, ……, $X_{O(n)}$, $Y_{O(n)}$	Observed values including errors
$X_{(A)}$, $Y_{(A)}$, ……, $X_{(n)}$, $Y_{(n)}$	The most probable computed values
$V_{(Xo(A))}$, $V_{(Yo(A))}$, …….. $V_{(Xo(n))}$, $V_{(Yo(n))}$	Residuals

This makes the observation equations flexible to deal with a great deal of problems and this can interpret the wide spread of using observation equations in almost all photogrammetric software to solve the co-linearity equations, co-planarity equations, and all models of 2D and 3D transformations. These equations can be arranged in algebraic matrixes system and solved using LSM, which is ideal and convenient for dealing with a big number of equations and suitable for computer calculations. Eqs. (3.1 to 3.6) and Eqs. (5.1 to 5.6) can be arranged in least squares matrixes as follows, and solved as shown:

$$A_{(n*m)} * X_{(m*1)} = L_{(n*1)} + V_{(n*1)} \quad (6)$$

$$X_{(m*1)} = (A^{T}_{(m*n)} * W_{(n*n)} * A_{(n*m)})^{-1} * (A^{T}_{(m*n)} * W_{(n*n)} * L_{(n*1)}) \quad (7)$$

Where,

n	The number of all observations (number of points * 4)
m	The number of unknowns (4 + number of points * 2)
A	Matrix of coefficients
A^T	Matrix transpose
W	Matrix of observations weights
X	Matrix of unknowns
L	Matrix of constant terms
V	Matrix of residuals

$$A = \begin{matrix} X(a) & -Y(a) & 1 & 0 & 0 & 0 & 0 & 0 & \dots & 0 & 0 \\ Y(a) & X(a) & 0 & 1 & 0 & 0 & 0 & 0 & \dots & 0 & 0 \\ X(b) & -Y(b) & 1 & 0 & 0 & 0 & 0 & 0 & \dots & 0 & 0 \\ Y(b) & X(b) & 0 & 1 & 0 & 0 & 0 & 0 & \dots & 0 & 0 \\ \dots & \dots & \dots & \dots & \dots & \dots & \dots & \dots & \dots & 0 & 0 \\ X(n) & -Y(n) & 1 & 0 & 0 & 0 & 0 & 0 & \dots & 0 & 0 \\ Y(n) & X(n) & 0 & 1 & 0 & 0 & 0 & 0 & \dots & 0 & 0 \\ 0 & 0 & 0 & 0 & 1 & 0 & 0 & 0 & \dots & 0 & 0 \\ 0 & 0 & 0 & 0 & 0 & 1 & 0 & 0 & \dots & 0 & 0 \\ 0 & 0 & 0 & 0 & 0 & 0 & 1 & 0 & \dots & 0 & 0 \\ 0 & 0 & 0 & 0 & 0 & 0 & 0 & 1 & \dots & 0 & 0 \\ \dots & \dots & \dots & \dots & \dots & \dots & \dots & \dots & \dots & 0 & 0 \\ 0 & 0 & 0 & 0 & 0 & 0 & 0 & 0 & \dots & 1 & 0 \\ 0 & 0 & 0 & 0 & 0 & 0 & 0 & 0 & \dots & 0 & 1 \end{matrix} \quad (8)$$

W = unite matrix with diagonal of weight value of each observation:

$$[wX_{(A)}\,;\, wY_{(A)}\,;\, wX_{(B)}\,;\, wY_{(B)}\,;\, \dots\dots\dots\dots;\, wX_{(n)}\,;\, wY_{(n)}\,;\, wX_{O(A)}\,;\, wY_{O(A)}\,;\, wX_{O(B)}\,;\, wY_{O(B)}\,;\, \dots\dots;\, wX_{O(n)}\,;\, wY_{O(n)}] \quad (9)$$

X = Vector matrix with one column of unknowns, including the 4 transformation parameters and the "true" values of X-Y system observations:

$$[a\,;\, b\,;\, T_{(N)}\,;\, T_{(E)}\,;\, X_{(A)}\,;\, Y_{(A)}\,;\, X_{(B)}\,;\, Y_{(B)}\,;\dots..;\, X_{(n)}\,;\, Y_{(n)}] \quad (10)$$

L = Vector matrix with one column of:

$$[E_{(A)}\,;\, N_{(A)}\,;\, E_{(B)}\,;\, N_{(B)}\,;\, \dots\dots\dots..;\, E_{(n)}\,;\, N_{(n)}\,;\, X_{O(A)}\,;\, Y_{O(A)}\,;\, X_{O(B)}\,;\, Y_{O(B)}\,;\, \dots..;\, \dots..;\, X_{O(n)}\,;\, Y_{O(n)}] \quad (11)$$

V = Vector matrix with one column of observations:

$$[V_{E(A)}\,;\, V_{N(A)}\,;\, V_{E(B)}\,;\, V_{N(B)}\,;\, \dots\dots\dots\dots,\, V_{E(n)}\,;\, V_{N(n)}\,;\, V_{(Xo(A))}\,;\, V_{(Yo(A))}\,;\, V_{(Xo(B))}\,;\, V_{(Yo(B))}\,;\, \dots..,\, \dots..,\, V_{(Xo(n))}\,;\, V_{(Yo(n))}] \quad (12)$$

2.1.5. LSM "Step 2"

Data Spoofing Method (DSM) and the similar techniques are appropriate for using in this stage after removing the majority of significant outliers in the RUNSAC steps, where these methods are designed to deal with observations including low percentage of outliers. In DSM, the covariance matrix of residuals of the 2D conformal transformation equations is determined, giving the standard deviation of residual of each observation. The residual of each observation is divided by its standard deviation, giving a specific value (*w*) for each observation. This value should fluctuate from 0 to 3, depending on the required confidence level. With 99% confidence level, the critical value is nearly 2.6 and with 99.99%, it is almost 3. Observations locates outside the specified ranges are considered as outliers with (100% - confidence level) probability of rejection the observation when it should be accepted (type 1 error). After removing outliers from observations, LSM can be applied again for getting the final model parameters. Eqs. (13) Shows the equations used in DSM to detect mismatched points form the LSM results.

$$CQ_{V(n*n)} = W^{-1}_{(n*n)} - A_{(n*m)} * (A^{T}_{(m*n)} * W_{(n*n)} * A_{(n*m)}) * A^{T}_{(m*n)} \quad (13)$$

The slandered deviation ($St_{V(1:n)}$) of observation residuals from (1 to n) is the rote square of the diagonal of matrix

$$CQV : St_{V.(1:n)} = [St_{V.E(A)}; St_{V.N(A)}; St_{V.E(B)}; St_{V.N(B)}; \ldots\ldots\ldots; St_{V.E(n)}; St_{V.N(n)}; St_{V.(Xo(A))}; St_{V.(Yo(A))}; St_{V.(Xo(B))}; St_{V.(Yo(B))}; \ldots\ldots\ldots; St_{V.(Xo(n))}; St_{V.(Yo(n))}] \quad (14)$$

$$w = [V_{E(A)}/St_{V.E(A)}; V_{N(A)}/St_{V.N(A)}; V_{E(B)}/St_{V.E(B)}; V_{N(B)}/St_{V.N(B)}; \ldots\ldots\ldots; V_{E(n)}/St_{V.E(n)}; V_{N(n)}/St_{V.N(n)}; V_{(Xo(A))}/St_{V.(Xo(A))}; V_{(Yo(A))}/St_{V.(Yo(A))}; V_{(Xo(B))}/St_{V.(Xo(B))}; V_{(Yo(B))}/St_{V.(Yo(B))}; \ldots\ldots\ldots; V_{(Xo(n))}/St_{V.(Xo(n))}; V_{(Yo(n))}/St_{V.(Yo(n))}] \quad (15)$$

2.2. 2D Affine Transformation-Based Filter (A-2DF)

Two-dimensional affine transformation is similar to conformal transformation with a slight modification to deal with different scale factors in the X & Y directions, and compensate for non-perpendicularity of the axis system. The affine transformation achieves these features by adding two additional unknowns to those used in conformal transformation to be six parameters, namely: scale in X direction, scale in Y direction, correction for non-perpendicularity, rotation angle, and 2D displacements. At least, three points must be known in both arbitrary and final coordinate systems to apply affine transformation model and find out the required six transformation parameters. Affine transformation is suitable for using in AIM, where shapes and scales in images change according to the capturing angles and the distance from camera centre to the different points forming the shape.

Affine transformation model can be carried out in four main steps: (1) scale change in X & Y directions, (2) correction for non-orthogonality, (3) rotation, and (4) 2D translation. For more precise results, the three points used in transformation procedure should be distributed in the image and chosen as far away from each other as possible. For more reliable and robust results, LSM can be used in affine transformation with more than three points, providing useful statistical testing information for detecting and removing outliers in observations. In AIM, affine transformation is applied using RUNSAC technique and the procedure is similar to that of conformal. Therefore, just the mathematical model of A-2DF using RUNSAC and followed by LSM for any number of points (n) are illustrated below without repeating the steps description: (All equations are after [4])

2.2.1. RUNSAC

Eqs (16.1 to 16.6) show the mathematical model of 2D affine transformation using the minimum number of observations required for determining the model parameters.

$$E_{(A)} = a_0 + a_1 * X_{(A)} + a_2 * Y_{(A)} \quad (16.1)$$

$$N_{(A)} = b_0 + b_1 * Y_{(A)} + b_2 * Y_{(A)} \quad (16.2)$$

$$E_{(B)} = a_0 + a_1 * X_{(B)} + a_2 * Y_{(B)} \quad (16.3)$$

$$N_{(B)} = b_0 + b_1 * Y_{(B)} + b_2 * Y_{(B)} \quad (16.4)$$

$$E_{(C)} = a_0 + a_1 * X_{(C)} + a_2 * Y_{(C)} \quad (16.5)$$

$$N_{(C)} = b_0 + b_1 * Y_{(C)} + b_2 * Y_{(C)} \quad (16.6)$$

Where,

$$\alpha = \tan^{-1}(-a_2 / b_2) \quad (17.1)$$

$$\varepsilon = \tan^{-1}(-b_1 / a_1) + \alpha \quad (17.2)$$

$$S_X = a_1 * (\cos(\varepsilon) / \cos(\varepsilon - \alpha)) \quad (17.3)$$

$$S_Y = b_2 * (\cos(\varepsilon) / \cos(\alpha)) \quad (17.3)$$

$$T_{(E)} = a_0 \quad (17.4)$$

$$T_{(N)} = b_0 \quad (17.5)$$

And,

$T_{(E)}$, $T_{(N)}$	Displacement parameters of 2D affine transformation
S_X, S_Y	Scale changing in X & Y directions
α	Rotation angle
ε	Nonorthogonality correction
$X_{(A)}$,$Y_{(A)}$,..., ..., $X_{(C)}$, $Y_{(C)}$	The coordinates of (A), (B) & (C) in X-Y coordinate system
$E_{(A)}$,$N_{(A)}$,..., ..., $E_{(C)}$, $N_{(C)}$	The coordinates of (A), (B) & (C) in E-N coordinate system

2.2.2. LSM

Following equations show 2D affine transformation observation equations with redundancy and LSM matrixes and all used parameters are as descried before:

$$E_{(A)} + V_{E(A)} = a_0 + a_1 * X_{(A)} + a_2 * Y_{(A)} \quad (18.1)$$

$$N_{(A)} + V_{N(A)} = b_0 + b_1 * X_{(A)} + b_2 * Y_{(A)} \quad (18.2)$$

$$E_{(B)} + V_{E(B)} = a_0 + a_1 * X_{(B)} + a_2 * Y_{(B)} \quad (18.3)$$

$$N_{(B)} + V_{N(B)} = b_0 + b_1 * X_{(B)} + b_2 * Y_{(B)} \quad (18.4)$$

$$E_{(C)} + V_{E(C)} = a_0 + a_1 * X_{(C)} + a_2 * Y_{(C)} \quad (18.5)$$

$$N_{(C)} + V_{N(C)} = b_0 + b_1 * X_{(C)} + b_2 * Y_{(C)} \quad (18.6)$$

$$E_{(n)} + V_{E(n)} = a_0 + a_1 * X_{(n)} + a_2 * Y_{(n)} \quad (18.7)$$

$$N_{(n)} + V_{N(n)} = b_0 + b_1 * X_{(n)} + b_2 * Y_{(n)} \quad (18.8)$$

$$X_{O(A)} + V_{(Xo(A))} = X_{(A)} \quad (18.9)$$

$$Y_{O(A)} + V_{(Yo(A))} = Y_{(A)} \quad (18.10)$$

$$X_{O(B)} + V_{(Xo(B))} = X_{(B)} \quad (18.11)$$

$$Y_{O(B)} + V_{(Yo(B))} = Y_{(B)} \quad (18.12)$$

$$X_{O(C)} + V_{(Xo(C))} = X_{(C)} \quad (18.13)$$

$$Y_{O(C)} + V_{(Yo(C))} = Y_{(C)} \quad (18.14)$$

$$X_{O(n)} + V_{(Xo(n))} = X_{(n)} \quad (18.15)$$

$$Y_{O(n)} + V_{(Yo(n))} = Y_{(n)} \quad (18.16)$$

Where,

$$A = \begin{bmatrix}
1 & X(A) & Y(A) & 0 & 0 & 0 & 0 & 0 & 0 & 0 & 0 & 0 & \ldots. & 0 & 0 \\
0 & 0 & 0 & 1 & X(A) & Y(A) & 0 & 0 & 0 & 0 & 0 & 0 & \ldots. & 0 & 0 \\
1 & X(B) & Y(B) & 0 & 0 & 0 & 0 & 0 & 0 & 0 & 0 & 0 & \ldots. & 0 & 0 \\
0 & 0 & 0 & 1 & X(B) & Y(B) & 0 & 0 & 0 & 0 & 0 & 0 & \ldots. & 0 & 0 \\
1 & X(C) & Y(C) & 0 & 0 & 0 & 0 & 0 & 0 & 0 & 0 & 0 & \ldots. & 0 & 0 \\
0 & 0 & 0 & 1 & X(C) & Y(C) & 0 & 0 & 0 & 0 & 0 & 0 & \ldots. & 0 & 0 \\
\ldots. & \ldots. & \ldots. & \ldots. & \ldots. & \ldots. & \ldots. & \ldots. & \ldots. & \ldots. & \ldots. & \ldots. & \ldots. & 0 & 0 \\
1 & X(n) & Y(n) & 0 & 0 & 0 & 0 & 0 & 0 & 0 & 0 & 0 & \ldots. & 0 & 0 \\
0 & 0 & 0 & 1 & X(n) & Y(n) & 0 & 0 & 0 & 0 & 0 & 0 & \ldots. & 0 & 0 \\
0 & 0 & 0 & 0 & 0 & 0 & 1 & 0 & 0 & 0 & 0 & 0 & \ldots. & 0 & 0 \\
0 & 0 & 0 & 0 & 0 & 0 & 0 & 1 & 0 & 0 & 0 & 0 & \ldots. & 0 & 0 \\
0 & 0 & 0 & 0 & 0 & 0 & 0 & 0 & 1 & 0 & 0 & 0 & \ldots. & 0 & 0 \\
0 & 0 & 0 & 0 & 0 & 0 & 0 & 0 & 0 & 1 & 0 & 0 & \ldots. & 0 & 0 \\
0 & 0 & 0 & 0 & 0 & 0 & 0 & 0 & 0 & 0 & 1 & 0 & \ldots. & 0 & 0 \\
0 & 0 & 0 & 0 & 0 & 0 & 0 & 0 & 0 & 0 & 0 & 1 & \ldots. & 0 & 0 \\
\ldots. & \ldots. & \ldots. & \ldots. & \ldots. & \ldots. & \ldots. & \ldots. & \ldots. & \ldots. & \ldots. & \ldots. & \ldots. & 0 & 0 \\
0 & 0 & 0 & 0 & 0 & 0 & 0 & 0 & 0 & 0 & 0 & 0 & 0 & 1 & 0 \\
0 & 0 & 0 & 0 & 0 & 0 & 0 & 0 & 0 & 0 & 0 & 0 & 0 & 0 & 1
\end{bmatrix}$$

W = unite matrix with diagonal of weight value of each observation:

$[wX_{(A)} ; wY_{(A)} ; wX_{(B)} ; wY_{(B)} ; wX_{(C)} ; wY_{(C)} ; \ldots\ldots\ldots; wX_{(n)} ; wY_{(n)} ; wX_{O(A)} ; wY_{O(A)} ; wX_{O(B)} ; wY_{O(B)} ; wX_{O(C)} ; wY_{O(C)} ; \ldots\ldots\ldots; wX_{O(n)} ; wY_{O(n)}]$ (19)

X = Vector matrix with one column of unknowns, including the 6 transformation parameters and the "true" values of X-Y system observations:

$[a_0 ; a_1 ; a_2 ; b_0 ; b_1 ; b_2 ; T_{(N)}; T_{(E)} ; X_{(A)} ; Y_{(A)} ; X_{(B)} ; Y_{(B)} ; X_{(C)} ; Y_{(C)} ; \ldots\ldots\ldots; X_{(n)} ; Y_{(n)}]$ (20)

L = Vector matrix with one column of:

$[E_{(A)} ; N_{(A)} ; E_{(B)} ; N_{(B)} ; E_{(C)} ; N_{(C)} ; \ldots\ldots\ldots; E_{(n)} ; N_{(n)} ; X_{O(A)} ; Y_{O(A)} ; X_{O(B)} ; Y_{O(B)} ; X_{O(C)} ; Y_{O(C)} \ldots\ldots\ldots; X_{O(n)} ; Y_{O(n)}]$ (21)

V = Vector matrix with one column of observations:

$[V_{E(A)} ; V_{N(A)} ; V_{E(B)} ; V_{N(B)} ; V_{E(C)} ; V_{N(C)} ; \ldots\ldots\ldots; V_{E(n)} ; V_{N(n)} ; V_{(Xo(A))} ; V_{(Yo(A))} ; V_{(Xo(B))} ; V_{(Yo(B))} ; V_{(Xo(C))} ; V_{(Yo(C))} \ldots\ldots\ldots; V_{(Xo(n))} ; V_{(Yo(n))}]$ (22)

The slandered deviation ($St_{V\,(1:\,n)}$) of residuals of observation from (1 to n) is the rote square of the diagonal of matrix $CQ_{V(n*n)}$:

$St_{V.\,(1:n)} = [St_{V.\,E(A)} ; St_{V.\,N(A)} ; St_{V.\,E(B)} ; St_{V.\,N(B)} ; St_{V.\,E(C)} ; St_{V.\,N(C)} ; \ldots\ldots\ldots; St_{V.\,E(n)} ; St_{V.\,N(n)} ; St_{V.\,(Xo(A))} ; St_{V.\,(Yo(A))} ; St_{V.\,(Xo(B))} ; St_{V.\,(Yo(B))} ; St_{V.\,(Xo(C))} ; St_{V.\,(Yo(C))} ; \ldots\ldots\ldots; St_{V.\,(Xo(n))} ; St_{V.\,(Yo(n))}]$ (23)

$w = [V_{E(A)}/St_{V.\,E(A)} ; V_{N(A)}/St_{V.\,N(A)} ; V_{E(B)}/St_{V.\,E(B)} ; V_{N(B)}/St_{V.\,N(B)} ; V_{E(C)}/St_{V.\,E(C)} ; V_{N(C)}/St_{V.\,N(C)} ; \ldots\ldots\ldots; V_{E(n)}/St_{V.\,E(n)} ; V_{N(n)}/St_{V.N(n)} ; V_{(Xo(A))}/St_{V.\,(Xo(A))} ; V_{(Yo(A))}/St_{V.\,(Yo(A))} ; V_{(Xo(B))}/St_{V.\,(Xo(B))} ; V_{(Yo(B))}/St_{V.\,(Yo(B))} ; V_{(Xo(C))}/St_{V.\,(Xo(C))} ; V_{(Yo(C))}/St_{V.\,(Yo(C))} ; \ldots\ldots\ldots; V_{(Xo(n))}/St_{V.\,(Xo(n))} ; V_{(Yo(n))}/St_{V.\,(Yo(n))}]$ (24)

2.3. Single Epipolar Geometry-Based Filter (S-EGF)

Beside 2D transformation methods, S-EGF is oftentimes used for detecting outliers in AIM results. Epipolar geometry is the geometry of stereo vision, which is based on photogrammetric co-planarity condition. When taking images of a 3D features from two different locations as seen in figure (3), a number of geometric relations between the object points (X), their 2D projections on the images (x_L & x_R), and the two cameras capturing centres (O_L & O_R) can be obtained. The

conversion of 3D sights to 2D views is referred to as a perspective projection, which can be modelled as 3D victors, starting from the camera optical centre, passing through the projection of the object on the image, and ending at the object point. As the capturing centres of the cameras are different, the projection of each camera centre can take a place on other camera's image plane as seen from figure (2), and these two points (e_L & e_R) are known as epipolar points. These two epipolar points lie on a single 3D line with the two optical centres of the two cameras. The left camera sees the line (O_L–X) as a point, where it is directly in line with that camera optical centre, whereas, from the right camera, the same line can be seen as the line (e_R–x_R). Correspondingly, the line (O_R–X) that can be seen as a point in the right camera appears as the line (e_L–x_L) in the left camera. These two lines (e_R–x_R) and (e_L–x_L) are known as the epipolar line of the right and lift images, respectively.

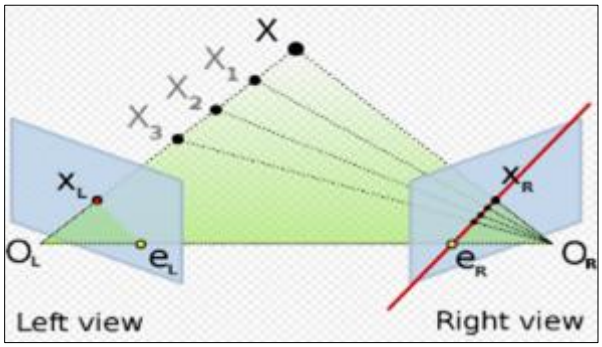

Figure 3 Epipolar Lines [2]

The epipolar plane includes seven main points: (X), (O_R & O_L), (x_R & x_L), and (e_R & e_L) and it can be described mathematically using just three points. In terms of lines, epipolar plane includes five main lines: (O_L–X), (O_R–X), (e_R–x_R), (e_L–x_L), and (O_L–O_R) and it can be mathematically described using just three lines. If the relative orientation parameters between the two cameras are fixed as in the case of ORN, this means that the 3D coordinates of the optical cameras centres and the 3D main rotations are known. Based on that, the coordinates of the two epipolar points on the two images can be determined. In S-EGF, the automatic matched points are rejected if the corresponding points do not lie on the epipolar lines of the two images. The mathematical model used in S-EGF is the photogrammetric co-planarity condition, showing in the following figure.

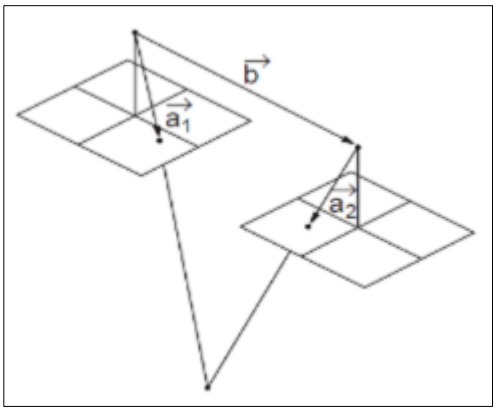

Figure 4 Co-planarity condition

From the figure, if the pair of rays defined by two corresponding image points and the base vector between the cameras perspective centers forms a plane in space, this means that the co-planarity condition is fulfilled. Mathematically, this is carried out by forcing these three vectors to be coplanar, which is in turn guaranteed by setting the triple scalar product to zero. The left vector (a1), the right vector (a2), the base vector (b), and the co-planarity condition (CC) are given by: (All equations are after [1])

$$a1 = \begin{bmatrix} D1 \\ E1 \\ F1 \end{bmatrix} = M1^T \begin{bmatrix} x1 - x0 \\ y1 - y0 \\ -f \end{bmatrix} \qquad (25) \qquad a2 = \begin{bmatrix} D2 \\ E2 \\ F2 \end{bmatrix} = M2^T \begin{bmatrix} x2 - x0 \\ y2 - y0 \\ -f \end{bmatrix} \qquad (26)$$

$$b = \begin{bmatrix} Bx \\ By \\ Bz \end{bmatrix} = \begin{bmatrix} XL2 - XL1 \\ YL2 - YL1 \\ ZL2 - ZL1 \end{bmatrix} \quad (27) \qquad CC = \begin{vmatrix} Bx & By & Bz \\ D1 & E1 & F1 \\ D2 & E2 & F2 \end{vmatrix} = 0 \quad (28)$$

$$CC = B_x (E_1 * F_2 - E_2 * F_1) + B_Y (F_1 * D_2 - F_2 * D_1) + B_Z (D_1 * E_2 - D_2 * E_1) = 0 \quad (29)$$

Where,

M1 & M2 The rotation matrix of the first and second images, respectively to be corresponding to the reference coordinate system, and in case of relative orientation, rotations in the first matrix are used as zeros and relative values are used for the relative rotations of the second image with respect to the first image.

x_1, y_1, x_2, y_2 The image coordinates of the same object on the two images.

f, x_0, y_0 The camera IOEs (focal length and the coordinates of camera optical centre on the image).

X_{L1}, Y_{L1}, Z_{L1} The coordinates of the first capturing station

X_{L2}, Y_{L2}, Z_{L2} The coordinates of the second capturing station

This filter is based on a clear mathematical model, which can be applied directly on the matched points for detecting outliers. As all parameters in the model are known, there is no need for estimating iterations, which means that nearly-real time outlier detection can be applied compared to the previous iterative techniques. On the other hand, this filter requires known relative orientation parameters between the two cameras, which are fixed in the case of ORN, but in the case of free-images matching, such parameters are almost unknowns. Moreover, initial threshold values are required for the mathematical model to accept or reject the observations. These thresholds are function of the EOP precision of the two cameras, the IOEs, and the image resolution, and these thresholds can be calculated using the theory of error distribution. The main limitation of this filter is its disability to deal with mismatched points, located on the extension of epipolar line. This type of mismatching is faced extensively when applying AIM in areas including features with similar horizontal lines. The effect of such environment increases in terrestrial photos when X-axes of the two images are parallel to these lines, where the epipolar lines on the images become parallel to the feature lines and as a results, detecting outliers along these lines becomes impossible. For proving the limitation of S-EGF mathematically, assume that the two images have the same X-axis, x0 & y0 = 0, and all rotations = 0, which means that B_Y and B_Z = 0 in equation (29), and the co-planarity condition becomes as following:

$$B_x (E_1 * F_2 - E_2 * F_1) = 0 \quad (30)$$

$$y1 * (- f) - y2 * (- f) = 0 \quad (31)$$

$$y1 = y2 \quad (32)$$

It is clear from equation (32) that the condition is effective only for detecting errors in y direction, and there is no way for dealing with errors in x direction, which is the main limitation of S-EGF.

2.4. Multi Epipolar Geometry-Based Filter (M-EGF)

As explained in the previous sections, C-2DF, A-2DF as well as S-EGF have their limitations in terms of processing time and disability of detecting outliers in specific and common environments. For this purpose, and due to the high sensitivity of the ORN based applications for mismatched points, there has been a need for developing another technique for providing the robots with precise, trusted, outlier-free, and real time matched points between images. M-EGF has been introduced and discussed by the author in [2, 3, 4] to overcome the limitations of the previous used filters. The idea of this filter is based on utilizing three cameras instead of two in robots, where three co-planarity conditions and three epipolar geometries will be formed as shown in figure (5). The three co-planarity equations can be written as following:

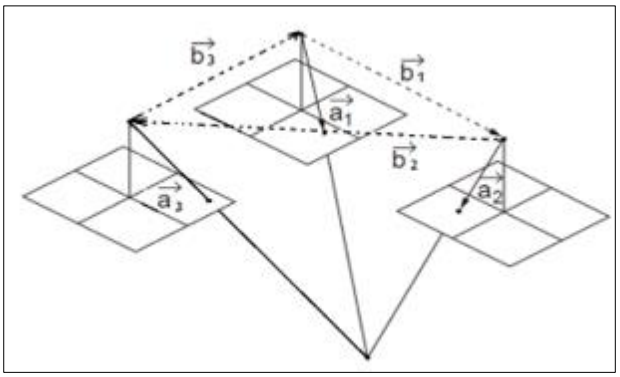

Figure 5 Multi-Epipolar lines and geometries [2]

Vector (a1), vector (a2), base vector (b1), and the co-planarity condition (CC1) are given by: (All equations are after [2, 3, 4])

$$a1 = \begin{bmatrix} D1 \\ E1 \\ F1 \end{bmatrix} = M1^T \begin{bmatrix} x1 - x0 \\ y1 - y0 \\ -f \end{bmatrix} \quad (33) \qquad a2 = \begin{bmatrix} D2 \\ E2 \\ F2 \end{bmatrix} = M2^T \begin{bmatrix} x2 - x0 \\ y2 - y0 \\ -f \end{bmatrix} \quad (34)$$

$$b1 = \begin{bmatrix} Bx12 \\ By12 \\ Bz12 \end{bmatrix} = \begin{bmatrix} XL2 - XL1 \\ YL2 - YL1 \\ ZL2 - ZL1 \end{bmatrix} \quad (35) \qquad CC1 = \begin{vmatrix} Bx12 & By12 & Bz12 \\ D1 & E1 & F1 \\ D2 & E2 & F2 \end{vmatrix} = 0 \quad (36)$$

$$CC1 = B_x12\ (E_1 * F_2 - E_2 * F_1) + B_Y12\ (F_1 * D_2 - F_2 * D_1) + B_Z12\ (D_1 * E_2 - D_2 * E_1) = 0 \quad (37)$$

Vector (a2), vector (a3), base vector (b2), and the co-planarity condition (CC2) are given by:

$$a2 = \begin{bmatrix} D2 \\ E2 \\ F2 \end{bmatrix} = M2^T \begin{bmatrix} x2 - x0 \\ y2 - y0 \\ -f \end{bmatrix} \quad (38) \qquad a3 = \begin{bmatrix} D3 \\ E3 \\ F3 \end{bmatrix} = M3^T \begin{bmatrix} x3 - x0 \\ y3 - y0 \\ -f \end{bmatrix} \quad (39)$$

$$b2 = \begin{bmatrix} Bx23 \\ By23 \\ Bz23 \end{bmatrix} = \begin{bmatrix} XL2 - XL3 \\ YL2 - YL3 \\ ZL2 - ZL3 \end{bmatrix} \quad (40) \qquad CC2 = \begin{vmatrix} Bx23 & By23 & Bz23 \\ D2 & E2 & F2 \\ D3 & E3 & F3 \end{vmatrix} = 0 \quad (41)$$

$$CC2 = B_x23\ (E_2 * F_3 - E_3 * F_2) + B_Y23\ (F_2 * D_3 - F_3 * D_2) + B_Z23\ (D_2 * E_3 - D_3 * E_2) = 0 \quad (42)$$

Vector (a3), Vector (a1), base vector (b3), and the co-planarity condition (CC3) are given by:

$$a3 = \begin{bmatrix} D3 \\ E3 \\ F3 \end{bmatrix} = M3^T \begin{bmatrix} x3 - x0 \\ y3 - y0 \\ -f \end{bmatrix} \quad (43) \qquad a1 = \begin{bmatrix} D1 \\ E1 \\ F1 \end{bmatrix} = M1^T \begin{bmatrix} x1 - x0 \\ y1 - y0 \\ -f \end{bmatrix} \quad (44)$$

$$b3 = \begin{bmatrix} Bx31 \\ By31 \\ Bz31 \end{bmatrix} = \begin{bmatrix} XL3 - XL1 \\ YL3 - YL1 \\ ZL3 - ZL1 \end{bmatrix} \quad (45) \qquad CC3 = \begin{vmatrix} Bx31 & By31 & Bz31 \\ D3 & E3 & F3 \\ D1 & E1 & F1 \end{vmatrix} = 0 \quad (46)$$

$$CC3 = B_x31\ (E_3 * F_1 - E_1 * F_3) + B_Y31\ (F_3 * D_1 - F_1 * D_3) + B_Z31\ (D_3 * E_1 - D_1 * E_3) = 0 \quad (47)$$

Where,

M3 The rotation matrix of the third image to be corresponding to the reference coordinate system, and in case of relative orientation, rotations in the first matrix are used as zeros and relative values are used for the rotations of the second and third images.

x_3, y_3 The image coordinates of the same object on the three images.

X_{L3}, Y_{L3}, Z_{L3} The coordinates of the third capturing station.

The rest As identified in section (3.3).

The work flow of this filter can be summarizing in the following steps:

- The three synchronized captured images are matched together using one of the common AIM techniques (Adjusted SURF in this paper) to find out the common corresponding points
- The co-planarity condition between each two images is applied, namely: CC1, CC2 & CC3
- If the three matched points between the three images have passed the three co-planarity conditions, this means that they are inliers and correctly matched.
- If the three matched points have failed to pass even one condition of the three conditions, the system will refuse the points and they are considered as outliers.

For proving the ability of M-EGF for detecting any mismatched points between the three images, assume that the three images have the same distribution shown in figure (6)

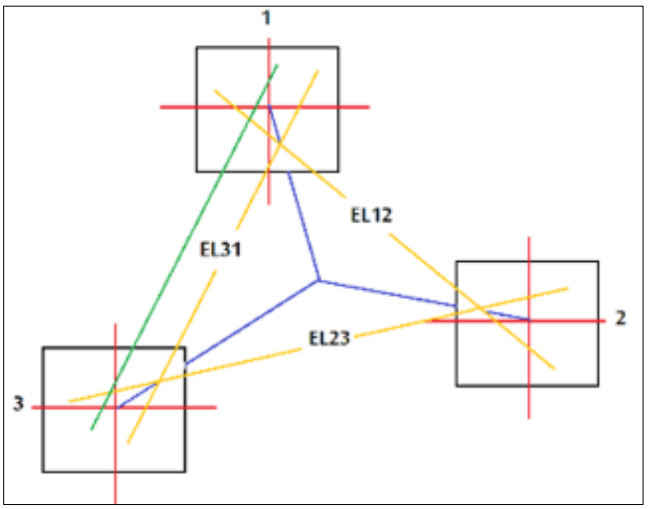

Figure 6 M-EGF

The S-EGF1 between image 1 & 2 is able to detect any mismatched points between the two images except those located on the extension of EL12 line. The same can be said for S-EGF2 & S-EGF3 and EL23 & EL31, respectively. If the mismatched points have passed the first filter (S-EGF1 for example) as the point located on the extension of EL12, the probability of this point to pass the other two filters is nearly zero, where the only passing case is when the error values of the mismatched point on EL12 and the mismatched point on EL23 guarantee the pseudo EL31 (the green line) to be parallel to the actual EL31 (the yellow line). Based on that, if precise values of the EOPs as well as IOEs for the three cameras are used, there will be no chance mathematically to accept any points when it should be rejected or rejected when it should be accepted [2, 3, 4].

3. Results & Discussion

To evaluate the performance of M-EGF, S-EGF, A-2DF and C-2DF, optical navigation based system that simulates ORN has been built. The system consists of 3 cameras connected to precise pulsing devise via distribution box. Precise electronic pulses are generated based on GPS time that obtained from built-in low-cost GPS receiver and then the pulses are distributed to the three cameras via the distribution box to guarantee taking the three images in the same time. Figure (7) shows the system and main components. The three cameras have been calibrated precisely using automatically detectable coded targets and Australis 7 software. Also, the relative EOPs of the three cameras have been determined using the same frame, where three simultaneous pictured from the three cameras have been taken for significant number of scaled coded targets and then applying AIM and SCBBA using Australis Software.

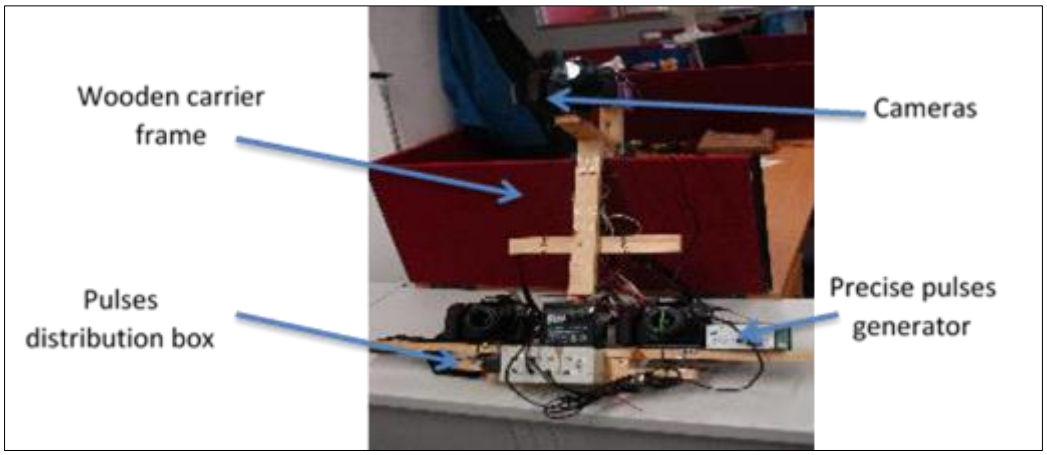

Figure 7 System designed by the author to evaluate MEGF, including: 3 cameras, precise pulses generator, pulses distribution box and wooden carrier frame [1]

For a good comparison, the system has been used to take simultaneous pictures in different AIM environments as illustrated in table (1). Figures (8), (9), (10), (11), (12), (13), (14), (15), & (16) show examples on the matching environments and examples on passed mismatched points for the different filters.

Table 1 The different image matching environment used in evaluation tests

No	Image matching environment
1	Limited DOF, rich in parallel lines & geometric features. Figure (8)
2	Medium DOF, with mixed and reflected features. Figure (9)
3	Open DOF, mixed features. Figure (10)
4	Limited DOF, rich in geometric, reflected and natural features. Figure (11)
5	Open DOF, rich in parallel lines & geometric features and moving items. Figure (12)
6	Confused DOF, rich in reflected features. Figure (13)
7	Limited DOF, with normal geometric, reflected features. Figure (14)
8	Limited DOF, with similar items & reflected features. Figure (15)
9	Difficult view angles with narrow DOF. Figure (16)

The evaluation technique used in this paper can be summarized in the following steps:

- A-2DF and C-2DF have been developed in Matlab using RANSAC and LSM, where the inputs are the matched points and some statistical thresholds and the results are two groups: inliers and outliers.
- S-EGF been developed in Matlab, where the inputs are the matched points, EOPs & IOEs of the two main cameras, and some statistical thresholds and the results are two groups: inliers and outliers.
- M-EGF also been developed in Matlab, where the inputs are the matched points, EOPs & IOEs of the three cameras, and some statistical thresholds and the results are two groups: inliers and outliers.
- The three images tacking in each environment have been automatically matched using adjusted SURF algorithm, taking the best 100 matched pints between each three images. This means that 900 matched points have been obtained between the three images and 2700 points in the 27 pictures used.
- These points have been manually and precisely checked and classified as correctly matched points (inliers) and incorrectly matched points (outliers)
- The lists of inliers and outliers have been used as inputs to the developed Matlab programmers to evaluate the performance of each filter, where each point is checked automatically for each filter and classified as inlier or outlier.

- The results of each filter are automatically compared to the manually classified lists, giving the error percentage of the accepted points that should be rejected (E%-AC), and the rejected points that should be accepted (E%-RJ).
- The processing time of each filter has been determined using Matlab.

Table (2) illustrates the error percentage of the accepted points that should be rejected (E%-AC), and the rejected points that should be accepted (E%-RJ) for the 4 filters in the different AIM shown in table (1). The averaged values of processing time of each filter have also been illustrated in table (2).

Table 2 (E%-AC), (E%-RJ), and processing time for the 4 filters in different AIM areas

Test No. See table (1)	C-2DF		A-2DF		S-EGF		M-EGF	
	E%-AC	E%-RJ	E%-AC	E%-RJ	E%-AC	E%-RJ	E%-AC	E%-RJ
1	18%	14%	13%	12%	15%	6%	0%	11%
2	48%	34%	35%	38%	6%	5%	0%	6%
3	Failed	Failed	Failed	Failed	12%	7%	0%	9%
4	26%	24%	27%	19%	9%	8%	0%	11%
5	Failed	Failed	Failed	Failed	15%	11%	0%	14%
6	Failed	Failed	56%	63%	7%	8%	0%	12%
7	33%	27%	26%	21%	4%	6%	0%	6%
8	29%	33%	22%	27%	5%	6%	0%	9%
9	Failed	Failed	Failed	Failed	12%	17%	0%	9%
Processing Time sec.	21.03		28.57		0.145		0.176	

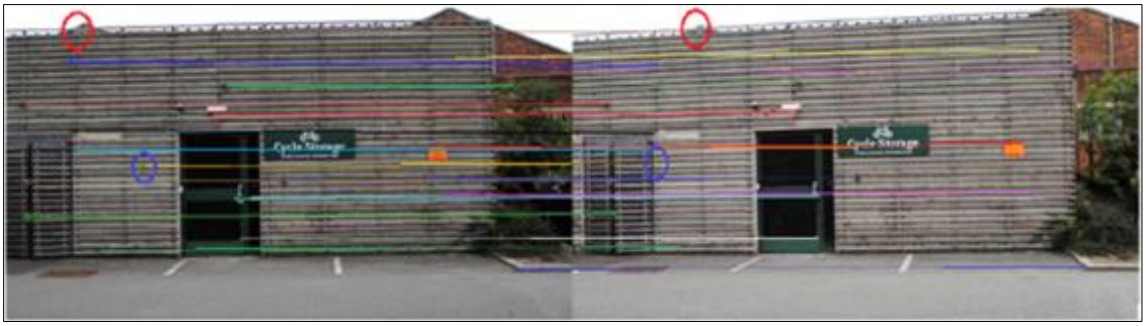

Figure 8 Limited DOF, rich in parallel lines & geometric features. Examples of some mismatched points passed from S-EGF

Figure 9 Medium DOF, with mixed and reflected features. Examples of some mismatched points passed from C-2DF & S-EGF

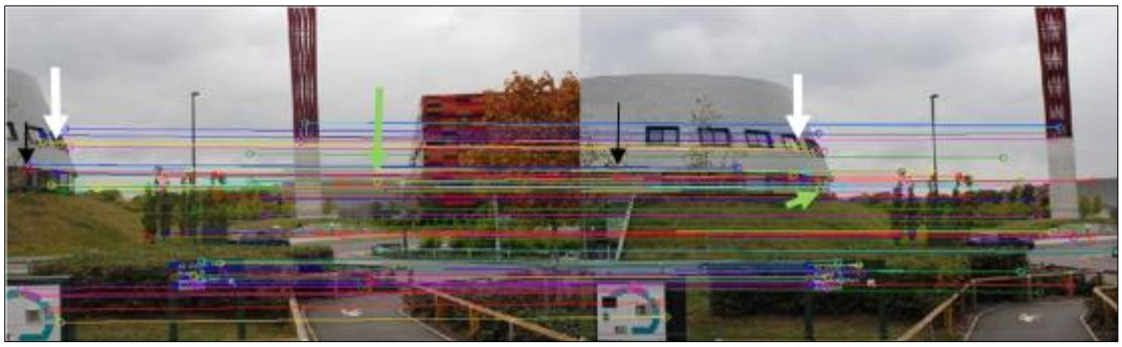

Figure 10 Open DOF, with mixed features. Examples of some mismatched points passed from A-2DF, C-2DF and S-EGF

Figure 11 Limited DOF, rich in geometric, reflected and natural features. Examples of some correctly matched points that rejected by C-2DF and A-2DF

Figure 12 Open DOF, rich in parallel lines & geometric features and moving items. Examples of some mismatched points passed from S-EGF

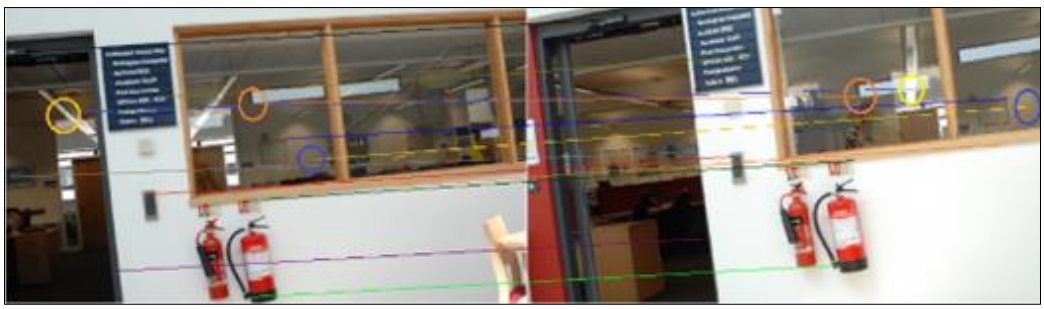

Figure 13 Confused DOF, rich in reflected features. Examples of some mismatched points passed from A-2DF, C-2DF and S-EGF

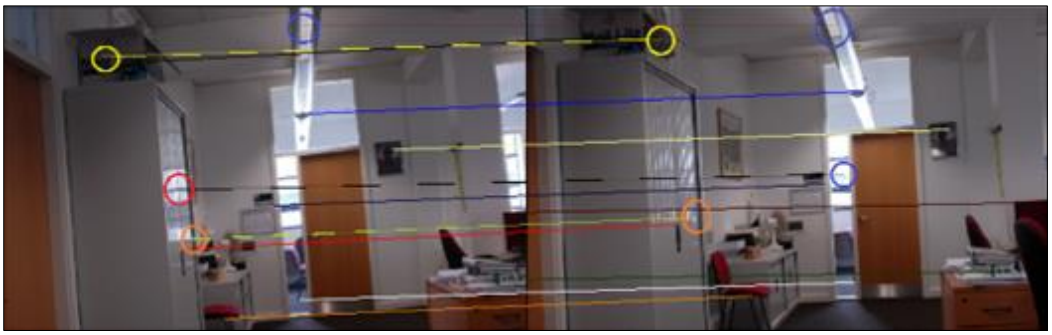

Figure 14 Limited DOF, normal geometric, reflected features. Examples of some mismatched points passed from A-2DF, C-2DF and S-EGF

Figure 15 Limited DOF, similar items & reflected features. Examples of some mismatched points passed from A-2DF, C-2DF and S-EGF

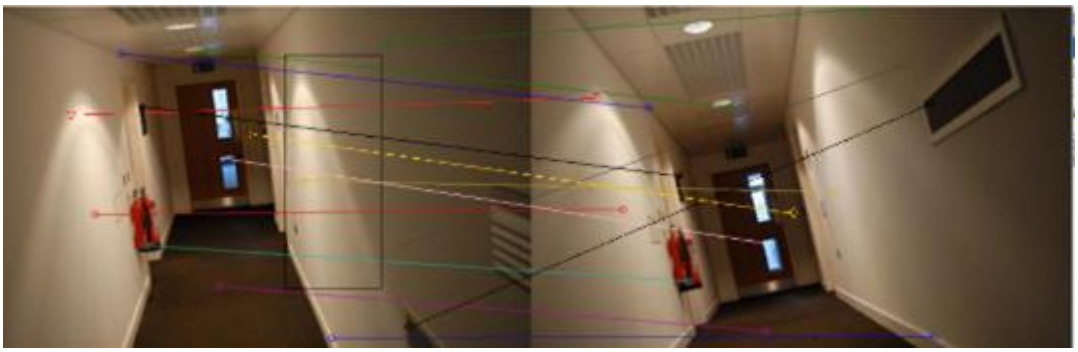

Figure 16 Difficult view angles with narrow DOF. Example of the high ability of M-EGF to provide trusted results

As clear from table (2), in areas with open, narrow, and confused DOF, both C-2DF and A-2DF have failed to deal with the inputted results of SURF algorithm. This means that RUNSAC and LSM did not be able to extract the right mathematical model based on these points. This can be attributed to the significant number of errors in the inputs and/or changing the relationships between the points on the two images significantly with changing the depth distance between points in optical direction when dealing with images that have open DOF. 2D-based filters have relatively worked well in areas with limited DOF where the relationships between points are nearly constant and the changes in scale, rotations and displacements can be considered in the mathematical models. Results show that A-2DF has the ability to filter out the mismatched points better that C-2DF, and this can be referred to the flexibility of the affine mathematical model to deal with figures that have different scales which is a common case when taking images from different optical angles. This might be clear in test (6), when evaluating the system with confused DOF, where C-2DF has failed to deal with the case, whereas A-2DF has succeed to get the mathematical model though the error percentages of accepted and rejected points are high compared to S-EGF and M-EGF. Furthermore, tests show that A-2DF and C-2DF are significantly affected by the complexity of the matching environment, where these filters are mainly based on extracting the right mathematical model that gathers the biggest group of matched points obtained from the matching technique. Increasing the number of mismatched points in the RANSAC inputs increases the difficulty of finding out the

correct geometric model, might give incorrect one, or fails to achieve any relationship. The other disadvantage of A-2DF and C-2DF is the long processing time that required to obtained the mathematical model and geometric parameters, where RUNSAC and LSM are iterative techniques and need to apply statistical testing for precise results. This makes such type of filters time consuming and may not be suitable for real time ORN based applications.

On the other hand, both S-EGF and M-EGF have shown high abilities to deal with all inputs from all AIM environments, regardless the percentage of errors and the number of mismatched points in SURF outputs. This can be attributed to the main dependency of these filters on fixed mathematical models and thus, there is no need for any estimations as in the case of C-2DF and A-2DF. Results show that DOF and the type and similarity of matching features do not have any effects on the performance of S-EGF and M-EGF, where these factors have an effect on the AIM technique and these filters are image points-independent models. From tables (1) and (2), it is clear that the performance of S-EGF is affected in areas that includes lines parallel to the cameras base line as in tests (1), (3) & (5) and figures (8), (10), & (12). This is referred to the disability of this filter to deal with mismatched points located on the extension of the epipolar line that includes the two corrected matched points. This can explain why there are error percentage in table (2) for point have been accepted when they should be rejected. As S-EGF uses a clear and fixed mathematical model, there is no reason logically for rejecting any corrected matched points. However, as clear from table (2), there are error percentage for rejection points when they should be accepted, which can be referred to the accuracy level of the cameras EOPs and IOEs that used in the co-planarity condition. The cameras used in the system and tests are non-metric cameras, which means that the IOEs are not stable and can change unsystematically after calibrations and this can affect the performance of the filter. The EOPs of the two cameras are also another main affected parameters, where the co-planarity equation is based considerably on the cameras positions and orientations. These EOPs have been determined precisely using the right technique and software as mentioned above, but keeping the cameras on the system handmade wooden frame without changing the EOPs is hard to be guaranteed. M-EGF has offered the best results in terms of providing filtered matched points without errors in all tests regardless the AIM environment or the number of errors in the inputted data. This, as explained in section (2.4), can be referred to the high restriction level of this filter, where the probability of the mismatched point to pass throughput the three co-planarity equations is nearly zero. The imprecision of the IOEs and the EOPs of the three cameras have also the reason for M-EGF to reject a number of corrected matched points when they should be accepted. From table (2), it is clear that the error percentage of the rejected points for this filter is higher than that of S-EGF and this can also be referred to the errors of the IOEs and EOPs in the co-planarity conditions which are applied three times on each point compared to once in S-EGF. Results illustrate that both S-EGF and M-EGF are timesaving, showing that M-EGF is the best filter for real time precise ORN applications. The high performance of M-EGF can open the doors for more integration levels with other different navigation techniques used in robots world, such as the integration with low-cost GPS receivers with different antenna types [13], the integration with low-cost GPS/MEMS-based INS [14, 15], the integration with enhanced stand-alone GPS by delta positioning [16, 17].

4. Conclusion

Results show that both C-2DF and A-2DF have failed to deal with the results of AIM in areas with open, narrow, and confused DOF due to changing the relationships between the points significantly with increasing the distances in optical direction. Also, both C-2DF and A-2DF have failed to find out the right mathematical model in data with high percentage of mismatched points and in cases of images with difficult view angles. With limited DOF and data with limited percentage of errors, E%-AC and E%-RJ of C-2DF and A-2DF have been higher than S-EGF and M-EGF, which reflects the weakness of using 2D transformation filters in precise and reliable ORN applications. The processing time is another limitation of C-2DF and A-2DF, where finding the right geometric model between hundreds of matched points is indeed time-consuming. Results show that A-2DF is relatively better than C-2DF due to its flexibility to deal with figures including different scales which is a common case when dealing with different levels of DOF and difficult capturing angles.

Tests show that S-EGF and M-EGF are timesaving and have a high ability to deal with any inputs, regardless DOF, view angle and the rate of gross errors in AIM outputs. This can be referred to the fixed mathematical models used in such filters, which cancel out the need of estimating any parameters. Tests show that S-EGF is affected in areas with lines parallel to the cameras base line, which reflects the disability of this filter to deal with mismatched points located on the extension of the epipolar line that includes the two matched points. Errors in the cameras EOPs and IOEs that used in the co-planarity condition have been reflected on the E%-RJ of S-EGF, where a small number of correctly matched points has been rejected when they should be accepted. Among the tested filters, M-EGF has offered the best results in terms of providing filtered error-free matched points in all tests. This can be referred to the high restriction level of this filter, where the probability for the mismatched point to pass throughput the three co-planarity equations is nearly zero. E%-AC of M-EGF is zero in all tests, which means that error-free observations can be provided to ORN from the outputs of

AIM techniques. The low quality of the IOEs and EOPs of the three cameras has been the reason behind rejection a small number of identical points when they should be accepted, which can be avoided with professionally manufactured robots and utilizing high quality cameras with stable IOEs. Tests show that M-EGF is a reliable, time-effective, error-free, and practical technique that meets the requirements of the high level, instantaneous, and precise ORN applications.

Compliance with ethical standards

Acknowledgments

I would like to express my special thanks to my friend Eng. Haytham alshatiti.

References

[1] McGlone JC, Mikhail EM, Bethel J, Roy M. Manual of photogrammetry. 5th ed. Bethesda, Md.: American Society of Photogrammetry and Remote Sensing; 2004.

[2] Amami M. Comparison Between Multi & Single Epipolar Geometry-Based Filters for Optical Robot Navigation. International Research Journal of Modernization in Engineering Technology and Science. March 2022; 4(3): 476-485.

[3] Amami M. Comparison between Multi Epipolar Geometry & Conformal 2D Transformation-Based Filters for Optical Robot Navigation. International Journal for Research in Applied Sciences and Engineering Technology. March 2022; 10(3): 388-398.

[4] Amami M. Comparison between Multi Epipolar Geometry & Affine 2D Transformation-Based Filters for Optical Robot Navigation. International Journal for Research in Applied Sciences and Engineering Technology. March 2022; 10(3): 399-409.

[5] Amami M. Low Cost Vision Based Personal Mobile Mapping System [Ph.D. dissertation]. University of Nottingham; 2015.

[6] Bayoud FA. Development of a Robotic Mobile Mapping System by Vision-Aided Inertial Navigation: A Geomatics Approach. [Ph.D. dissertation]. University of Calgary; 2006.

[7] Amami MM, Smith MJ, Kokkas N. Low Cost Vision Based Personal Mobile Mapping System. ISPRS- International Archives of The Photogrammetry, Remote Sensing and Spatial Information Sciences. 2014; XL-3/W1: 1-6.

[8] Amami, M. Speeding up SIFT, PCA-SIFT & SURF Using Image Pyramid. Journal of Duhok University, [S.I]. July 2017; 20(1): 356-362.

[9] Lowe D. Distinctive Image Features from Scale-Invariant Key points, IJCV. 2004; 60(2): 91-110.

[10] Juan L, Gwun O. A comparison of SIFT, PCA-SIFT and SURF. International Journal of Image Processing (IJIP). 2009; 3: 143-152.

[11] Bay H, Tuytelaars T, Van Gool L. SURF: Speeded Up Robust Features. 9th European Conference on Computer Vision. 2006; 404-417.

[12] Amami M. Fast and Reliable Vision-Based Navigation for Real Time Kinematic Applications. International Journal for Research in Applied Sciences and Engineering Technology. Feb 2022; 10(2): 922-932.

[13] Amami, M. Testing Patch, Helix and Vertical Dipole GPS Antennas with/without Choke Ring Frame. International Journal for Research in Applied Sciences and Engineering Technology. Feb. 2022; 10(2): 933-938.

[14] Amami M. The Integration of Time-Based Single Frequency Double Differencing Carrier Phase GPS/ Micro-Elctromechanical System-Based INS. International Journal of Recent Advances in Science and Technology. Dec 2018; 5(4): 43-56.

[15] Amami, M. Enhancing Stand-Alone GPS Code Positioning Using Stand-Alone Double Differencing Carrier Phase Relative Positioning. Journal of Duhok University (Pure and Eng. Sciences). 2017; 20(1): 347-355.

[16] Amami M. The Integration of Stand-Alone GPS Code Positioning, Carrier Phase Delta Positioning & MEMS-Based INS. International Research Journal of Modernization in Engineering Technology and Science. March 2022; 4(3): 700-715.

[17] Amami M. The Advantages and Limitations of Low-Cost Single Frequency GPS/MEMS-Based INS Integration. Global Journal of Engineering and Technology Advances. Feb. 2022; 10(2): 018-031.